18th International Conference
ENGINEERING MECHANICS 2012
Svratka, Czech Republic, May 14 – 17, 2012

pp. 1611–1620
Paper #194

INDIRECT DETERMINATION OF MATERIAL MODEL PARAMETERS FOR SINGLE TRABECULA BASED ON NANOINDENTATION AND THREE-POINT BENDING TEST

P. Zlámal*, O. Jiroušek, D. Kytýř, T. Doktor**

Abstract: *The aim of the paper is to develop a procedure for determination of elasto-visco-plastic constitutive model with damage for human single trabecula. The procedure is suited for indirect establishing of material model based on nanoindentation and three-point bending test. Constants of the material model are identified by Finite Element (FE) simulations and curve fitting using an algorithm based pn least squares fitting of the experimental curves. In the case of nanoindentation, the penetration depth of tip during the FE analyses (FEA) is fitted to experimental nanoindentation curves. In the case of three-point bending, displacements of nodes are compared with displacements of markers observed during the experiment using digital image correlation.*

Keywords: ***elasto-visco-plastic-damage model, FEM, trabecular bone, three-point bending***

1. Introduction

A single trabecula is the basic beam-shaped element of bone structure and knowledge of mechanical properties at this level is important for understanding of overall deformation behaviour of bone tissue as well as for simulation of osteoporotic changes. Recently, one of the powerful methods used to measure the elastic properties of samples at microscale level is nanoindentation. Nanoindentation is usually used for determination of elastic properties of material, whereas yield properties as well as softening behaviour can not be directly measured. On the other hand, mechanical testing (tension test, three-point bending test etc.) is often carried out to describe nonelastic deformation behaviour. In this study an elasto-visco-plastic constitutive model with damage for human single trabecula was developed using two different procedures including experimental tests and FEA. First procedure is based on nanoindentation and inverse FE modelling. During the procedure the numerical results were fitted to experimental indentation curves to obtain nonelastic constants of material model. In the second procedure a three-point bending is performed and the constants are identified from displacement of nodes in FEA. Displacements of nodes of numerical model are compared with displacements of markers observed experimentally using digital image correlation (DIC) technique.

2. Materials and Methods

2.1. Nanoindentation test

For nanoindentation test a 3mm thick sample was cutted from human (72-year male) femoral head using precision saw (Isomet 1000, Buehler GmbH, Germany). The sample was delipidated in 1% Alconox (Alconox detergent, Alconox Inc., USA) detergent lotion in ultrasonic bath (Sonic 3, Polsonic, Poland) for 15 minutes and then rinsed with distilled water. The temperature of the bath has not exceeded 40°C. In our test an indentation depth during nanoindentation was approximately 1 μm, therefore it was necessary reduce the surface roughness of the sample to a minimal possible value. For this reason the

*Ing. Petr Zlámal: Czech Technical University in Prague, Faculty of Transportation Sciences; Konviktská 20;110 00; Prague; CZ; e-mail: xzlamal@fd.cvut.cz

**Doc. Ing. Ondřej Jiroušek, PhD., Ing. Daniel Kytýř PhD., Ing. Tomáš Doktor: Institute of Theoretical and Applied Mechanics, v.v.i., Academy of Sciences of the Czech Republic; Prosecká 76; 190 00; Prague; CZ; e-mail: {jirousek, kytyr, doktor}@itam.cas.cz

cleaned sample was embedded into a low shrinkage epoxy resin (EpoxyCure, Buehler GmbH, Germany) and grinded using polishing machine (LaboPol-4, Struers, Denmark) with diamond grinding discs (grain sizes: 35 μm and 15 μm) and monocrystalline diamond suspensions (9 μm, 3 μm, 1 μm). Final polishing was performed by aluminium-oxide suspension (Al_2O_3) with grain size 0.05 μm. Average surface roughness achieved using the procedure was 25 nm [Kytyr (2011)].

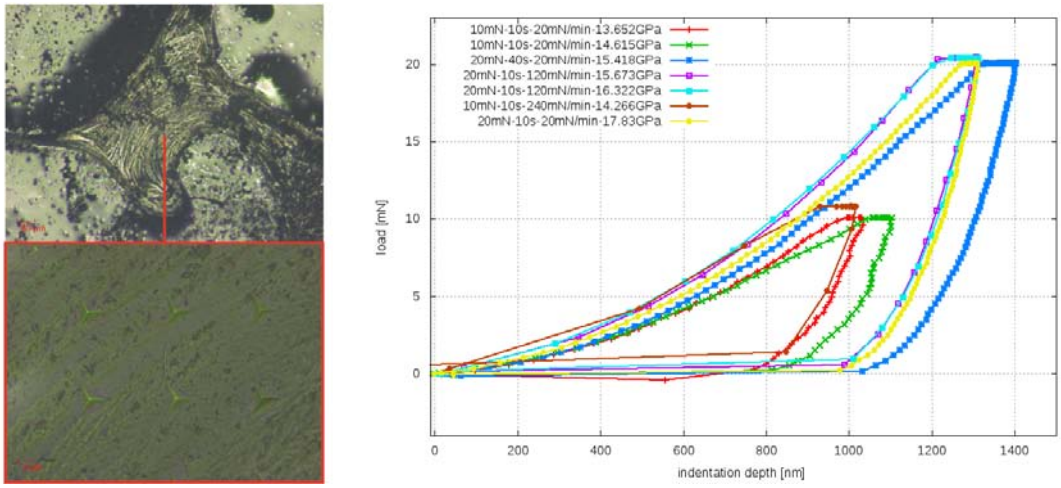

Fig. 1: Trabecular bone indentation area with grid of indents (left), selected indentation curves for FEA (description of legend: peak force - holding time - loading rate - Young's modulus) (right)

During the nanoindentation the applied force and penetration depth of diamond indenter (Berkovich tip) were measured. For statistically significant FEM fitting procedure of nanoindentation test multiple indents (approximately 300) with two peak forces ($10, 20$ mN), three holding times ($10, 20, 40$ s) and loading rates ($20, 120, 240$ mN/min) were performed. The indents were made with 10 μm grid size (Fig. 1-left). Young's modulus was determined directly from nanoindentation curves (Fig. 1-right) by Oliver-Pharr method [Oliver and Pharr (1992)]:

$$\frac{1}{E_r} = \frac{1-\nu^2}{E} + \frac{1-\nu_i^2}{E_i} \tag{1}$$

where E_i, ν_i is Young's modulus and Poisson's ratio of the diamond tip; E, ν is Young's modulus and Poisson's ratio of the specimen (ν is expertly estimated). Reduced modulus E_r can be calculated:

$$E_r = \frac{\sqrt{\pi}}{2}\frac{S}{\sqrt{A}}, \qquad S = \frac{dP}{dh} \tag{2}$$

where A is the projected area of elastic contact , S is stiffness of the upper portion of the unloading data, P is applied load and h is penetration depth. Obtained values of Young's modulus for selected indentation curves for FEA are shown in the legend of Fig. 1-right.

2.2. Numerical simulation of nanoindentation test

For FE simulations of the nanoindentation test a rotationally axisymmetric plane model was used. The Berkovich indenter (three sided pyramid) was replaced with a cone with equivalent contact surface [Lucchini (2011)]. For better numerical convergence the sharp tip of the cone is usually rounded $100 \div 300$ nm. Radius 200 nm was chosen based on the study of Chen (2009). The FE model (see Fig. 2) was composed from 13,806 2-D structural solid elements (6,997 nodes) with linear shape function and contact elements inserted between the model of indenter and the specimen. For the indenter a pure elastic material model with Young's modulus E_i =1140 GPa and Poisson's ratio $\mu_i = 0.07$ was applied. For the model of trabecular bone elasto-visco-plastic material model with damage was used. From experimental indentation curves, especially from the shape during the unloading phase, the necessity to use damage model was apparent. Usage of the damage model was a logical step to extend the elasto-plastic material model previously published in Jirousek (2011). For the considered model it is necessary to identify 10 material constants:

- two elastic constants: Young's modulus ($\mathbf{E}$) and Poisson's ratio ($\boldsymbol{\nu}$)
- two constants for plasticity with von Mises yield criterion and bilinear isotropic hardening: yield point ($\boldsymbol{\sigma_y}$) and tangent modulus ($\mathbf{E_{tan}}$)
- four constants ($\mathbf{C_1}$, $\mathbf{C_2}$, $\mathbf{C_3}$, $\mathbf{C_3}$) for implicit creep with time hardening according to the equation:

$$\dot{\varepsilon}_{cr} = C_1 \sigma^{C_2} t^{C_3} e^{-C_4/T} \tag{3}$$

where $\dot{\varepsilon}_{cr}$ is the change in equivalent creep strain with respect to time, σ is the equivalent stress, t is the time at end of substep and T is the temperature

- constants ($\mathbf{D_1}$,$\mathbf{D_2}$) for damage model published in Zhang (2010):

$$E_{new} = (1 - d_c) E_0 \tag{4}$$

$$d_c = D_1 (1 - e^{-D_2 \cdot \varepsilon_{eqa}^{pl}}) \tag{5}$$

where E_{new} is the degradated Young's modulus of the element which is calculated at the end of each loadstep, E_0 is the initial Young's modulus of the element and ε_{eqa}^{pl} is the accumulated equivalent plastic strain in the element at the end of loadstep according to:

$$\varepsilon_{eqa}^{pl} = \sum \Delta\varepsilon_{eq}^{pl} \tag{6}$$

$$\begin{aligned} \Delta\varepsilon_{eq}^{pl} = \frac{\sqrt{2}}{3}[(\Delta\varepsilon_x^{pl} - \Delta\varepsilon_y^{pl})^2 + (\Delta\varepsilon_y^{pl} - \Delta\varepsilon_z^{pl})^2 + (\Delta\varepsilon_z^{pl} - \Delta\varepsilon_x^{pl})^2 \\ + \frac{3}{2}(\Delta\gamma_{xy}^{pl^2} + \Delta\gamma_{yz}^{pl^2} + \Delta\gamma_{xz}^{pl^2})]^{\frac{1}{2}} \end{aligned} \tag{7}$$

where $\varepsilon_x, \varepsilon_y, \cdots$ are appropriate strain components. Equation 7 is derived from von Mises equation:

$$\varepsilon_{eq} = \frac{1}{\sqrt{2}(1+\nu')}[(\varepsilon_x - \varepsilon_y)^2 + (\varepsilon_y - \varepsilon_z)^2 + (\varepsilon_z - \varepsilon_x)^2 + \frac{3}{2}(\gamma_{xy}^2 + \gamma_{yz}^2 + \gamma_{xz}^2)]^{\frac{1}{2}} \tag{8}$$

where ν' is the effective Poison's ratio and in case of plastic deformation it is $\nu' = 0.5$.

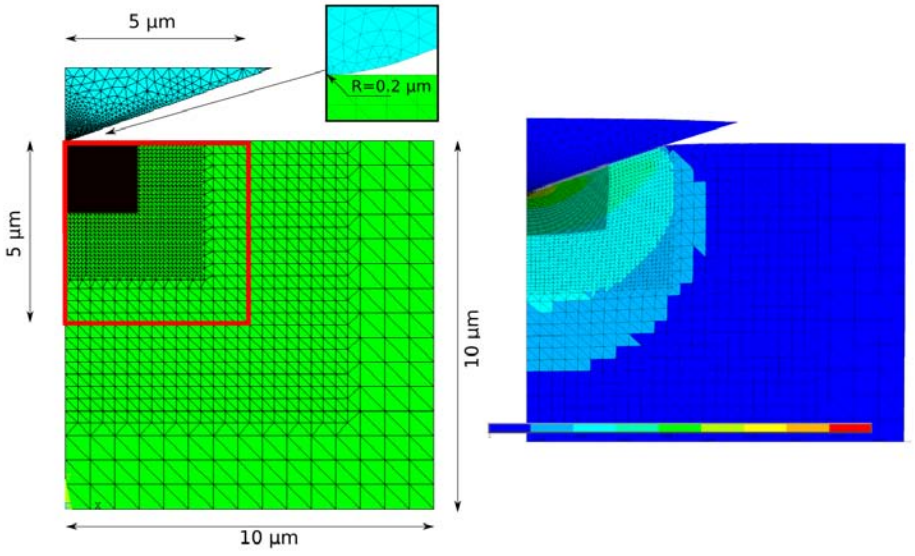

Fig. 2: FE model of nanoindentation with damage model application zone (red box)(left), equivalent plastic strain distribution (right)

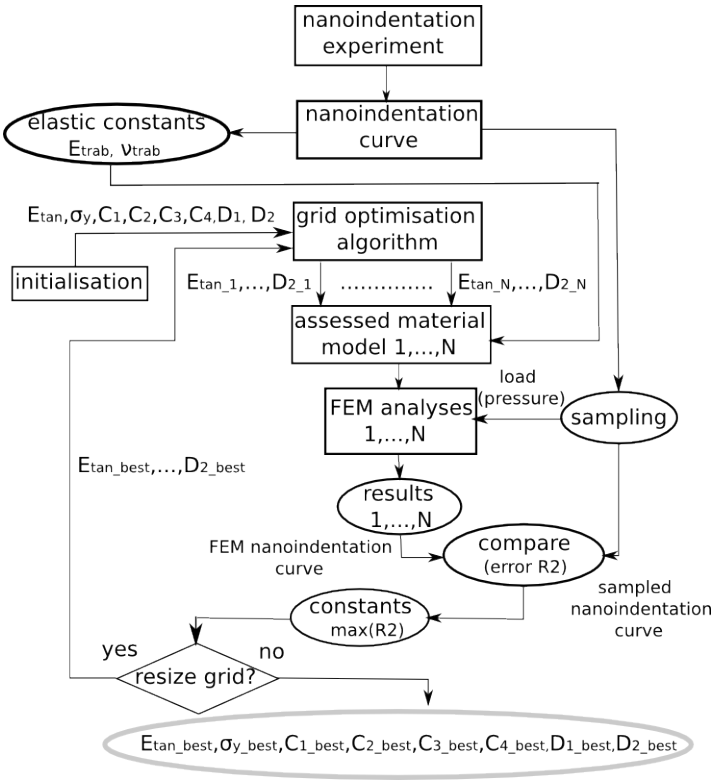

Fig. 3: Flowchart of the algorithm for material constants optimization

The size of the damage model application zone was determined according to nonzero equivalent plastic strain values obtained during the analyses. Equivalent plastic strain distribution caused by $20\,\mathrm{mN}$ peak force and the size of damage zone are shown in Fig 2.

Material constants (except the elastic constants which were determined directly from experiment) were identified using FEA of the nanoindentation test. Nanoindentation curves were sampled and load values were applied to model of the indenter in each loadstep. Resulting penetration depths were compared to experimentally obtained ones by least squares method and R^2 error was calculated. Initial values of material constants were modified in each simulation using custom grid optimisation algorithm (described in the flowchart in Fig. 3) to minimalize R^2.

2.3. Three-point bending test

Samples of trabeculae were extracted under magnifying glass (4 x magnification) from the same proximal human femur (Fig. 4) as in the case of the nanoindentation using a sharp-tip scalpel and pair of tweezers. Trabeculae were cleaned off marrow and grease in a detergent in an ultrasonic bath.

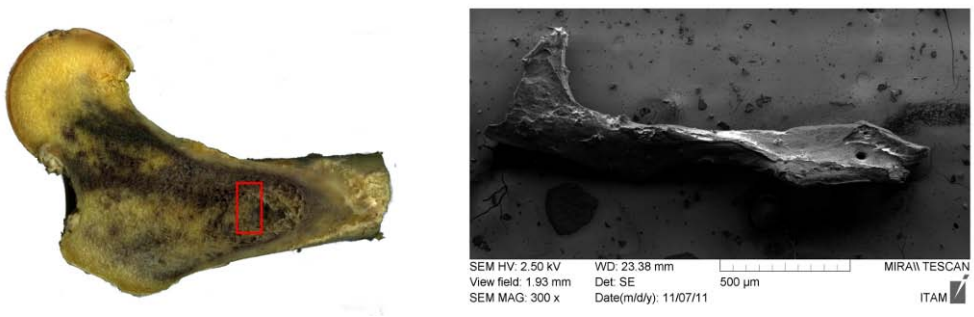

Fig. 4: Cross-section of human femur with harvesting area (left), single trabecula captured by SEM (right)

For three-point bending test an experimental setup (Fig. 5) composed from translation stages (Standa Ltd., Lithuania) was developed. Loading is controlled by steeper motor (SX16, Microcon, Czech Republic) and the load is applied using a precision linear stage (M-UMR3.5, Newport Corp., USA) with differential micrometer (DM11-5, Newport Corp., USA) with $0.1\ \mu\mathrm{m}$ sensitivity and $5\ \mathrm{mm}$ travel range. Applied force is measured using $2.2\ \mathrm{N}$ load sensor (FBB350, FUTEK Advanced Sensor Technology Inc., USA). For optical measurement of deformations the setup is equipped with a CCD camera (CCD 1300-F, VDS Vosskuhler GmbH, Germany) with 1280x1024 px resolution attached to an optical microscope (Navitar Inc., USA). This configuration enables to acquire images of deformation behaviour of

Fig. 5: Experimental setup (left), CCD camera capturing (middle), detail of the loading area (right)

the single trabecula during the bending test. Groups of markers were selected in the captured image data (Fig. 6-left) and their position were tracked using DIC toolkit [Jandejsek (2010)] based on Lucas-Kanade algorithm. During the tracking it is possible that correlation is lost in some of the markers (significant change in the brightness of the pixel in an image due to reflections, blur, large movement etc.). The markers with lost correlation are automatically identified and eliminated from further strain calculation. Loss of the correlation for one marker is shown in Fig. 6-bottom left and marked by a green circle. From the identified vertical displacements (Fig. 6-right) of middle span markers (6,7,8), strain values were determined according to equation for flexural strain of simply supported beam:

$$\varepsilon_f = \frac{6uh}{l^2} \tag{9}$$

where u is the average deflection of mid-span markers, h is the trabecula height in place of the applied load and l is the length between the supports.

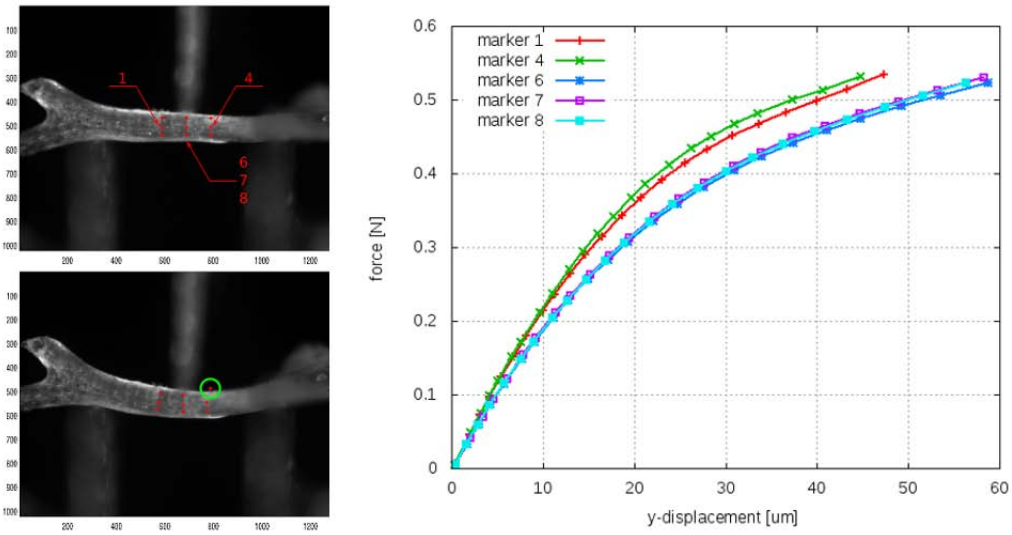

Fig. 6: Deflection of the single trabecula with group of markers (left), displacements of markers during the bending test (right)

For stress calculation, moment of inertia of the sample in the mid-span and the measured force were used. Young's modulus and the yield stress were established from stress-strain curve by the 0.2%

offset method [McNamara (2006)]. For estimation of measurement errors a precision of the setup was evaluated for materials with known properties, namely for BoPET film (Biaxially-oriented polyethylene terephthalate, DuPont, USA) and for Co-Ni wire. Overall precision of measurement was determined as upper limit of all measurement: Young's modulus 5% and yield stress 7% [Zlamal (2011)].

2.4. Numerical simulation of three-point bending test

For numerical simulation of the three-point bending test it is necessary to develop accurate geometrical model of the single trabecula. To facilitate this, each trabecular sample was mounted on a rotational stage and 360 images (with 1° step size) were captured using the CCD camera. The shape-from-silhouette method based on inverse Radon transform [Pintavirooj (2002)] was employed for geometrical model development. The volumetric model was created from the reconstructed data based on marching cubes algorithm [Lorensen (1987)] and segmentation techniques using our in-house segmentation and modelling software [Vavrik (2010)]. Volumetric model was meshed and exported to general purpose FE software Ansys (v12.1, Ansys Inc., USA). Example of the developed FE model of trabecula is shown in Fig. 7. The FE model of trabecula was composed from 3-D 10-nodes tetrahedral elements with quadratic

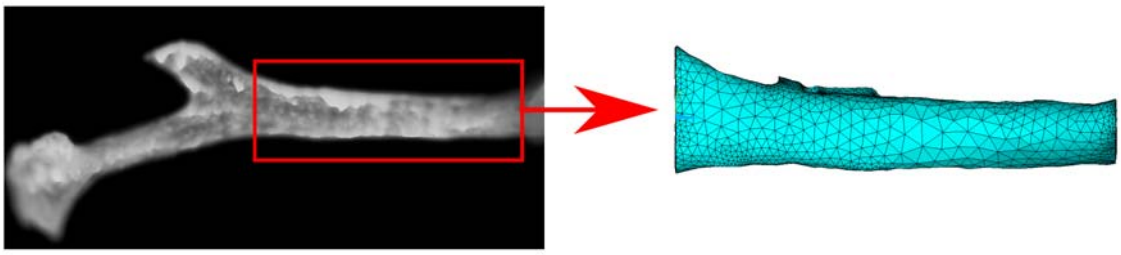

Fig. 7: The FE model development: captured image (left), final FE model (right)

shape functions. Nodes corresponding with position of correlation markers were selected on the surface of the model and the same boundary conditions as in the experiment were applied. To simulate the bending test, the same material model for the single trabecula as in case of the nanoindentation was used. In contrast to identification from the nanoindentation test, elastic constants (Young's modulus and Poisson's ration) were also identified. All ten constants were varied using the modified algorithm (described in Fig. 3) and resulting displacements of nodes were compared with displacements of the markers. The best set of material constants was determined based on R^2 error calculation.

3. Results and discussions

From the nanoindentation experiment, only the elastic constants were directly identified. Remaining constants for the elasto-visco-plastic material model with damage were identified using FEA of the nanoindentation test. For the statistically significant results, the emphasis was given to variety of control parameters (peak forces, holding times, loading rates) in the set (n=6) of curves for the FEA. Resulting constants were found using minimizing error based on least squares method in the optimization procedure and are shown in Tab. 1. A comparison of nanoindentation curves for the experiment and the FEA for the resulting constants are shown in Fig. 8-left. From the results it is evident that some constants have standard deviations larger than 20%, namely σ_y, C_1, C_3, D_2. This deviation may be due to several aspects, e.g: (i) the trabecular bone is biological material and its material properties are site-dependent. The indentation curves used in FEA were obtained from various indentation matrix, consequently, on various trabeculae; (ii) different material model sensitivity on identified constants. The second assumption was tested by sensitivity study.

The sensitivity study was performed for one indent and resulting curves are shown in Fig. 9. From the curves we can make following assumptions: (i) from graph for yield point it is obvious that the sensitivity is decreases with increasing σ_y value and for values above $100\,\mathrm{MPa}$ the changes between the curves are minimal. Small changes of curves in observed range $100 \div 300\,\mathrm{MPa}$ are the reason for relatively large deviation (24.3%) for the resulting mean value $\sigma_y = 180\,\mathrm{MPa}$; (ii) values of C_1 should

Tab. 1: Resulting constants from the nanoindentation of human trabecular bone

	mean value	standard deviation
Young's modulus [GPa]	15.39	1.4 (9.1%)
Poisson's ratio [-]	0.2[1]	-
σ_y [MPa]	180	43 (24.3%)
E_{tan} [MPa]	1854	336 (18.1%)
C_1 [-]	3.1e-18	4.08e-18 (135%)
C_2 [-]	6.1	0.42 (6.9%)
C_3 [-]	0.88	0.71 (80.7%)
C_4 [-]	0	-[2]
D_1 [-]	0.73	0.037 (5.1%)
D_2 [-]	25.3	7.48 (29.4%)

[1] expertly determined

[2] not varied

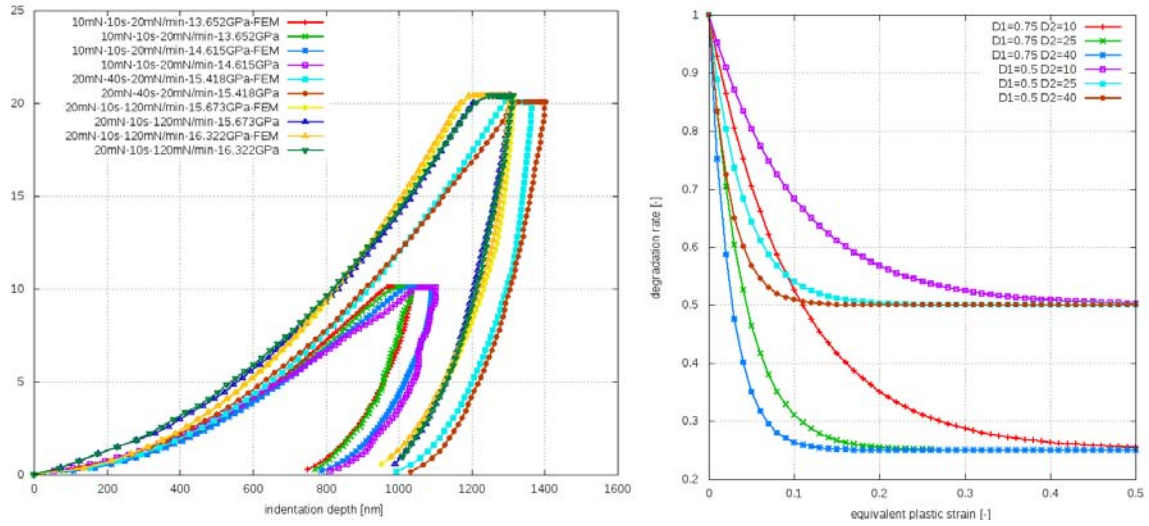

Fig. 8: Resulting nanoindentation curves for the best set of constants (left), damage variable as a function of the equivalent strain for variable values of D_1 and D_2

be varied in range up to order e-18. Lower values have no effect on the FEM curves. After exclusion of the low values (lower than $1 \cdot$ e-18), standard deviation was decreased to 2.06e-18$\pm$9.72e-19 (48%); (iii) constant C_2 is useful varied up to 6.5, higher values produced large creep which was not observed during the experiment; (iv) from equation 3 and graph in Fig. 9 (row 3, column 1) it is evident that constant C_3 has significant effect only for values larger than 1.9. Identified resulting value 0.88$\pm$0.71 is lower than this threshold and its influence for the material model is insignificant; (v) insensitivity to constant C_4 in varied range confirms zero effect of temperature creep during the FEA and C_4 constant can not be varied; (vi) the damage model as a function of the equivalent strain depends on variables D_1 and D_2 and this dependency is shown in Fig. 8-right. Constant D_1 determines the maximum degradation rate and constant D_2 governs the rate which degradation approaches this limiting value. The influence of these constants on the nanoindentation curve is predictable and shown in Fig. 9 (row 4, column 1 and 2). For increasing values of D_1 and D_2 increased penetration depth for the same value of load was observed.

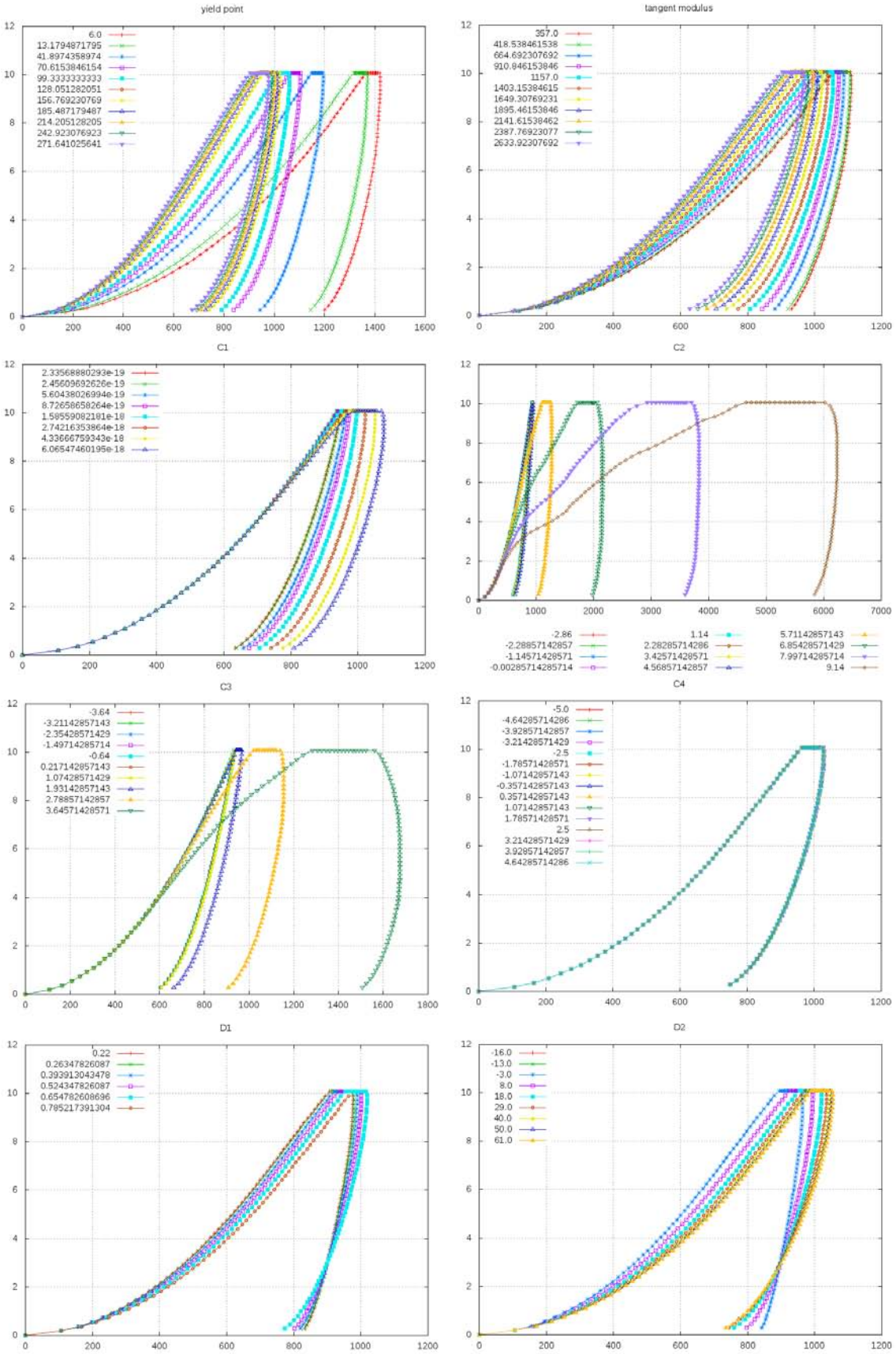

Fig. 9: Sensitivity study

Tab. 2: Resulting constants from the three-point bending test of human trabecular bone

	exp:mean value	exp:STD	FEM:mean value	FEM:STD
Young's modulus [GPa]	9.34	1.36 (14.5%)	12.093	0.727 (6%)
Poisson's ratio [-]	-	-	0.2	0.05 (24%)
σ_y [MPa]	185.6	42 (22.6%)	170	4.96 (2.9%)
E_{tan} [MPa]	-	-	1924	263 (13%)
C_1 [-]	-	-	8.6e-18	5.1e-18 (59.4%)
C_2 [-]	-	-	4.7	0.88 (18.6%)
C_3 [-]	-	-	2.1	0.67 (32.7%)
C_4 [-]	-	-	0	-
D_1 [-]	-	-	0.52	0.08 (16%)
D_2 [-]	-	-	30.1	1.4 (4.6%)

From the three-point bending test of the single trabecula Young's modulus and yield stress were directly determined. The experimental results, namely displacements of correlation markers and the applied force were used for FEA with goal to identify the constants for a material model same as in case of the nanoindentation. Resulting constants is shown in Tab. 2 and the comparison of displacements of the markers for the experiment and FEA are shown in Fig. 10-left, final distribution of vertical displacements is shown in Fig. 10-right. Experimentally measured values of Young's modulus for the single trabecula in the case of the nanoindentation and three-point bending were 15.3 ± 1.4 GPa and 9.34 ± 1.36 GPa, respectively. Difference in values can be explained by the nature of experiments, the nanoindentation measurement of elastic properties is very localised and depend on place of indent. Usual procedure is to indent a polished sample not necessarily taken perpendicularly to the longitudinal axis of trabecula and thus measured elastic constants can be significantly different. It was shown by Brennan (2009) that Young's modulus measured by nanoindentation can vary in the cross-section of a trabecula in 5 GPa range. On the other hand, Young's modulus measured by three-point bending is expected to the average of values measured by nanoindentation in the cross-section. Second aspect is related to place of harvesting that was not the exactly same.

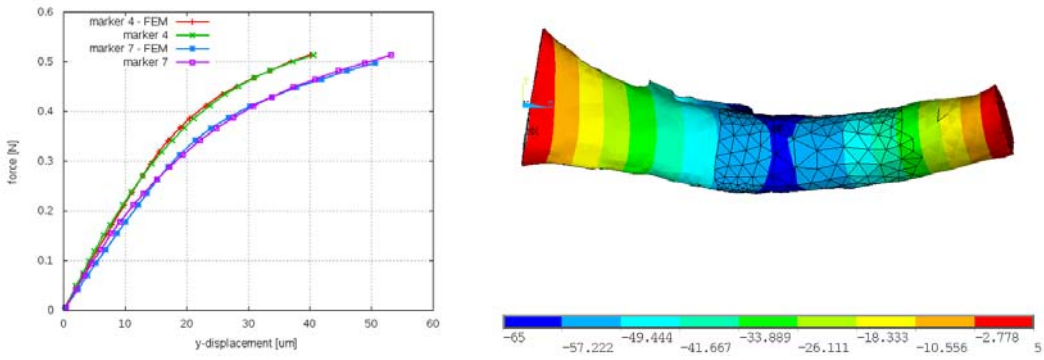

Fig. 10: Comparison of displacements of markers (left), distribution of vertical displacements

4. Conclusions

In this study elasto-visco-plastic material model with damage for the human single trabecula based on the nanoindentation test and three-bending test using the very similar procedure was established. Results

from FE simulation of experiments were fitted to experimentally measured values. Measured dependencies during the nanoindentation and three-point bending were force-penetration depth and force-displacements of the markers, respectively. From the numerical fitting procedure, the constants of material model were identified. Some of the constants can be directly determined from experiments. In the case of the nanoindentation the Young's modulus was 15.39 ± 1.4 GPa and in the case of the three-point bending test the Young's modulus and the yield stress were 9.34 ± 1.36 GPa and 185.64 ± 42 MPa, respectively. The visco-plastic constants and constants for the damage model were assessed from inverse FE modelling in both experiments. Young's modulus (E=12.093 ± 0.72 GPa) and yield stress (170 ± 4.96 MPa) were also determined by numerical analyses but only for the three-bending test. Influence of individual constants were investigated using sensitivity analysis of the nanoindentation test. The study confirms the possibility of using the indirect determination of the numerical material model for single trabecula based on FEM and experimental methods (nanoindentation and the micromechanical testing).

Acknowledgments

The research has been supported by the Grant Agency of the Czech Republic (grant no. P105/10/2305), Czech Technical University (grant no. SGS11/140/OHK2/2T/16), RVO: 68378297 and research plan of Ministry of Education and Sports (MSM 6840770043).

References

Kytyr, D., Doktor, T., Valach, J., et al. (2011), Evaluation of sample preparation procedures for micro-mechanical testing of trabecular bone. In: *10th Youth Symposium on Experimental Solid Mechanics* (M. Stockmann et al). Chemnitz University of Technology, Chemnitz, pp 71-72.

Oliver, W. C. and Pharr, G. M. (1992), An improved technique for determining hardness and elastic modulus using load and displacement sensing indentation experiments. *Journal of Materials Research, Cambridge Univ Press*, Vol 7, No.6, pp 1564-1583.

Jirousek, O., Nemecek, J., Kytyr, D., et al. (2011), Nanoindentation of Trabecular Bone – Comparison with Uniaxial Testing of Single Trabecula, *Chemicke listy, Ceska spolecnost chemicka*, Vol. 105, No.17, pp 668-671.

Lucchini, R., Carnelli, D., Ponzoni M., et al. (2011), Role of damage mechanics in nanoindentation of lamellar bone at multiple sizes: Experiments and numerical modeling. *Journal of the Mechanical Behavior of Biomedical Materials, Elsevier Ltd.*, Vol 4, No.8, pp 1852-1863.

Chen, Ch. (2009), 2-D finite element modeling for nanoindentation and fracture stress analysis. *PhD Thesis, University of South Florida*

Zhang, J., Michalenko, M. M., Kuhl, E., et al. (2010), Characterization of indentation response and stiffness reduction of bone using a continuum damage model. *Journal of the mechanical behavior of biomedical materials, Elsevier Ltd*, Vol 3, No.2, pp 189-202.

Zlamal, P., Jirousek, O. (2011), Parameter estimation of material model for single trabecula from micromechanical testing. *Chemicke listy, Ceska spolecnost chemicka*, article in press.

Jandejsek, I., Valach, J., Vavrik, D. (2010), Optimization and Calibration of Digital Image Correlation Method. *Experimentalni analyza napeti 2010* (Smid, P.). Univerzita Palackeho v Olomouci, Olomouc, pp 121-126.

McNamara L.M., Ederveen, A.G.H., Lyons C.G., et al. (2006), Strength of cancellous bone trabecular tissue from normal, ovariectomized and drug-treated rats over the course of ageing. *Bone, Elsevier Ltd*, Vol 39, No.2, pp 392-400.

Pintavirooj, C., Sangworasil, M. (2002), 3d-shape reconstruction based on radon transform with application in volume measurment. *The 10-th International Conference in Central Europe on Computer Graphics, Visualization and Computer Vision'2002*, Pilsen, Czech Republic.

Lorensen, W. E., Cline, H. E. (1987), Marching Cubes: A high resolution 3D surface construction algorithm. *Computer Graphics*, Vol. 21, No. 4, pp 163-169.

Vavrik, D., Dammer J., Jakubek, J., et. al. (2010), Advanced X-ray radiography and tomography in several engineering applications. *Nuclear Instruments and Methods in Physics Research Section A: Accelerators, Spectrometers, Detectors and Associated Equipment, Elsevier Ltd*, Vol 633, Supplement 1, pp 152-155.

Brennan, O., Kennedy, O.D., Lee, T.C., et al. (2009), Biomechanical properties across trabeculae from the proximal femur of normal and ovariectomised sheep. *Journal of Biomechanics, Elsevier Ltd*,Vol 42, No.4, pp 498-503. 42(4):498-503.